arXiv:1608.07211v1 [physics.atom-ph] 25 Aug 2016

Dynamics of atomic spin-orbit-state wave packets produced by short-pulse laser photodetachment

S. M. K. Law and G. F. Gribakin*

Center for Theoretical Atomic, Molecular and Optical Physics,

School of Mathematics and Physics,

Queen's University Belfast, Belfast BT7 1NN, United Kingdom

Abstract

We analyse the experiment by Hultgren *et al.* [Phys. Rev. A **87**, 031404 (2013)] on orbital alignment and quantum beats in coherently excited atomic fine-structure manifolds produced by short-pulse laser photodetachment of C^-, Si^- and Ge^- negative ions, and derive a formula that describes the beats. Analysis of the experimental data enables us to extract the non-coherent background contribution for each species, and indicates the need for a full density matrix treatment of the problem.

PACS numbers: 32.80.Rm, 32.80.Gc

* g.gribakin@qub.ac.uk

I. INTRODUCTION

In this paper we analyse the dynamics of quantum wave packets produced by coherent excitation of atomic fine-structure manifolds in laser photodetachment experiments, and probed by multiphoton ionization. We show that for atoms with $np^2\ {}^3P$ ground state the corresponding signal has a very specific shape, which we determine analytically and find to be in good agreement with experiment.

The development of laser pulses of few-femtosecond duration allows one to resolve the electron motion in valence shells of atoms and molecules in the time domain (see, e.g., [1–6]). Recently 100 fs pulse pump-probe experiments [7, 8] were carried out to investigate the dynamics induced by the spin-orbit interaction in neutral atoms. In these experiments C, Si and Ge atoms with outer np^2 configuration were prepared in the ^3P ground state by photodetachment of the respective half-filled valence shell negative ions ($np^3\ {}^4S$) by a linearly polarized pump pulse. Upon interaction with the infrared laser pulse, the emission of p electrons with orbital angular momentum projection $m = 0$ is strongly favoured in comparison to $m = \pm 1$. This causes the formation of a state with an electron density hole localized along the pump laser polarization axis and constitutes the orbital alignment effect. Such a state is not an eigenstate of the atomic Hamiltonian when the spin-orbit interaction is included, but a superposition of the fine-structure levels ^3P_J, which evolves in time according to the energy splittings in this manifold. This means that even for a light atom, such as C, the relativistic spin-orbit interaction is essential in determining the electron dynamics following the pump pulse. In Refs. [7, 8] this effect was probed by applying a time-delayed ionizing probe pulse and measuring the signal of ionized electrons for parallel and perpendicular polarization of the pump and probe pulses, as a function of the time delay.

The experimental findings demonstrated the dependence of the ionization yield on the time-varying hole density and the presence of quantum beat oscillations of the signal with the delay time for C and Si (with no distinct signal for Ge). This showed that electron dynamics resulting from the spin-orbit interaction could be observed for both lighter and heavier atoms. In a recent paper [9] Rey and van der Hart used R-matrix theory with time dependence (RMT) to model the experiment of Refs. [7, 8]. They calculated the electron spectra following ionization of carbon in the initial orbitally-aligned states with magnetic

quantum numbers $M_L = 0$ and 1, and observed significant differences between these two cases, matching the experimental findings. They also considered the evolution of the fine-structure-state wave packet with the pump-probe delay time and simulated the experimental signal by integrating electron emission within the cone of 11.7 degrees around the polarization direction of the probe pulse with momenta $p \geq 0.4$ a.u. The scaled normalized yield obtained in this way was found to be in good agreement with the experimental data from Ref. [8].

In the present work we show that the experimental results can be described in a much simpler manner. We use the assumption (similar to that used in Ref. [9] and key to the experimental method of Refs. [7, 8]) that removal of $m = 0$ electrons dominates both the photodetachment (pump) and subsequent photoionization (probe), and consider the motion of the $np^2\ ^3P$ fine-structure wave packet in C, Si, or Ge. This gives a simple analytical expression for the signal as a function of the pump-probe time delay. In order to make comparisons with experimental results of Ref. [7] we scale the signal to account for the background counts that could be present under the experimental conditions. This allows us to analyse the contribution of background to the observed signal beats and to effectively describe the loss of coherence in the wave packets for systems with short beat periods.

The structure of the paper is as follows. In Sec. II we derive the expression that describes the beats of the signal due to the time evolution of the atomic-state wave packet. In Sec. III we use our analytical expression to model the experimental data and compare with the phenomenological simulation used in Refs. [7, 8]. Section IV provides brief conclusions. Note that we use atomic units throughout.

II. THEORY

Before the arrival of the pump pulse the negative ions are in the $np^3\ ^4S$ ground state with the total orbital angular momentum $L = 0$ and spin $S = 3/2$, and their projections $M_L = 0$ and $M_S = -3/2, \ldots, 3/2$. The total angular momentum and its projection are $J = S$ and $M = M_S$.

We assume that after an instantaneous photodetachment of an electron with $m = 0$, the atoms are produced in a $np^2\ ^3P$ state at zero time delay, after which this state evolves according to the energy splittings of the fine-structure manifold. The initial state of the atom is described by its total orbital and spin angular momentum quantum numbers L

and S with projections M_L and M_S, respectively, which we denote by $|L, M_L; S, M_S\rangle$ (or a superposition of such states, see below). In the LS-coupling scheme, the time evolution of the initial atomic state $|L, M_L; S, M_S\rangle$ is given by

$$|\Psi(t)\rangle = \sum_J e^{-iE_J t} C^{JM}_{LM_L SM_S} |J, M\rangle \,, \tag{1}$$

where $|J, M\rangle$ is the fine-structure energy eigenstate with the total angular momentum J, projection $M = M_L + M_S$, and energy E_J, $C^{JM}_{LM_L SM_S}$ denotes a Clebsch-Gordan coefficient, and $|\Psi(0)\rangle = |L, M_L; S, M_S\rangle$.

To find the occupancies of the electron orbitals with $m = 0$ in $|\Psi(t)\rangle$, which determine the ionization signal after the probe pulse, we expand the fine-structure states $|J, M\rangle$ in the basis of LS states $|L, M_L; S, M_S\rangle$ (see the Appendix for the explicit form of these in terms of the single-particle states),

$$|\Psi(t)\rangle = \sum_J \sum_{M'_L, M'_S} e^{-iE_J t} C^{JM}_{LM_L SM_S} C^{JM}_{LM'_L SM'_S} |L, M'_L; S, M'_S\rangle \,, \tag{2}$$

where the second sum is over all M'_L and M'_S such that $M'_L + M'_S = M$.

The removal of an $m = 0$ electron from the initial $M_S = 3/2$ anion state produces the atomic state $|1, 0; 1, 1\rangle$. The subsequent time evolution of the atomic wave packet is found by applying Eq. (2) and evaluating the appropriate Clebsch-Gordan coefficients,

$$|\Psi_1(t)\rangle = \frac{1}{2}(e^{-iE_2 t} + e^{-iE_1 t}) |1, 0; 1, 1\rangle + \frac{1}{2}(e^{-iE_2 t} - e^{-iE_1 t}) |1, 1; 1, 0\rangle \,. \tag{3}$$

The corresponding ionization signal after the probe pulse is proportional to the probability of finding an $m = 0$ electron in the state (3),

$$S^{(1)}_{\parallel} = \frac{1}{2}(1 - \cos\omega_{21} t), \tag{4}$$

$$S^{(1)}_{\perp} = \frac{1}{4}(3 + \cos\omega_{21} t), \tag{5}$$

for the parallel and perpendicular polarization of the probe, respectively. Here $\omega_{JJ'} = E_J - E_{J'}$, and the explicit forms of the atomic states given in the Appendix were used.

The removal of an $m = 0$ electron from the initial $M_S = 1/2$ anion state produces a superposition of atomic states,

$$\frac{1}{\sqrt{3}} |1, 0; 1, 1\rangle + \sqrt{\frac{2}{3}} |1, 0; 1, 0\rangle \,, \tag{6}$$

(see the Appendix), whose time evolution is given by

$$|\Psi_2(t)\rangle = \frac{1}{\sqrt{3}}|\Psi_1(t)\rangle + \sqrt{\frac{2}{3}}\left(\frac{2}{3}e^{-iE_2t} + \frac{1}{3}e^{-iE_0t}\right)|1,0;1,0\rangle$$
$$+ \sqrt{\frac{2}{3}}\left(\frac{1}{3}e^{-iE_2t} - \frac{1}{3}e^{-iE_0t}\right)(|1,1;1,-1\rangle + |1,-1;1,1\rangle). \quad (7)$$

This gives the probabilities of finding an $m = 0$ electron at time t as

$$S_{\parallel}^{(2)} = \frac{1}{6}(1 - \cos\omega_{21}t) + \frac{8}{27}(1 - \cos\omega_{20}t), \quad (8)$$
$$S_{\perp}^{(2)} = \frac{1}{12}(7 + \cos\omega_{21}t) + \frac{1}{27}(5 + 4\cos\omega_{20}t). \quad (9)$$

Note that since the Clebsch-Gordan coefficient C^{10}_{1010} is zero, no interference is observed between the $J = 0$ and $J = 1$ sublevels. This is in agreement with the experimental analysis [7, 8], which allowed for the presence of the $\omega_{10} = E_1 - E_0$ beat frequency, but found its contribution statistically insignificant. Note also that the sum $S_{\parallel}^{(i)} + 2S_{\perp}^{(i)} = 2$, independently of time, which could be expected since there are two orthogonal directions perpendicular to the polarization of the pump pulse.

The total signals for the parallel and perpendicular polarizations of the pump and probe pulses are proportional to $S_{\parallel} = S_{\parallel}^{(1)} + S_{\parallel}^{(2)}$ and $S_{\perp} = S_{\perp}^{(1)} + S_{\perp}^{(2)}$. (The initial anion states with $M_S = -3/2$ and $-1/2$ give the identical contribution.) The normalized electron yield measured in the experiment is

$$S(t) = \frac{S_{\perp} - S_{\parallel}}{S_{\perp} + S_{\parallel}}. \quad (10)$$

Using Eqs. (4), (5), (8), and (9), and allowing for a constant time shift t_0 related to the uncertainty of the zero time delay [8], and for some signal background that may contribute to $S_{\parallel}$ and $S_{\perp}$, we obtain

$$S(t) = \frac{\frac{5}{9} + \cos[\omega_{21}(t - t_0)] + \frac{4}{9}\cos[\omega_{20}(t - t_0)] + \Delta S_b}{\frac{67}{27} - \frac{1}{3}\cos[\omega_{21}(t - t_0)] - \frac{4}{27}\cos[\omega_{20}(t - t_0)] + S_b}, \quad (11)$$

where S_b and ΔS_b are the sum and difference of the background contributions for the parallel and perpendicular polarizations. Such background can also account for reduced coherence of the wave packet when the pump pulse duration becomes comparable to or greater than the beat periods (see Sec. III). Note that a better quantity than that in Eq. (10) would probably be the ratio $(2S_{\perp} - S_{\parallel})/(2S_{\perp} + S_{\parallel})$, in which the denominator should be constant.

The contribution of the oscillating terms in the denominator of Eq. (11) is relatively small, even in the absence of any background S_b. This means that $S(t)$ is close to a simple linear combination of a constant and two beat components with frequencies ω_{21} and ω_{20}. Equation (11) shows that the relative contribution of the beats with frequencies ω_{21} and ω_{20} is fixed, and the beat period between the higher-lying levels $J = 1, 2$ gives the dominant contribution. Note also that Eq. (11) with $\Delta S_b = S_b = 0$ predicts a positive constant offset $\overline{S} = 15/67 \sim 0.2$, which is qualitatively similar to the observations (see Sec. III).

In analysing the experimental data, the authors of Refs. [7, 8] used the following phenomenological function

$$f(t) = c_0 + \alpha_1 \cos[\omega_{21}(t - t_0)] + \alpha_2 \cos[\omega_{20}(t - t_0)] + \alpha_3 \cos[\omega_{10}(t - t_0)], \tag{12}$$

with five fitting parameters: a constant offset c_0, amplitudes α_i ($i = 1, 2, 3$) of all three possible beats with frequencies ω_{21}, ω_{20}, and ω_{10}, and t_0.

The beat frequencies are determined by the corresponding energy splittings [10]: $\omega_{21} =$ 5.086, 27.510, and 160.65 ps^{-1}, $\omega_{20} =$ 8.175, 42.028, and 265.56 ps^{-1}, and $\omega_{10} =$ 3.089, 14.524, and 104.95 ps^{-1}, for C, Si, and Ge, respectively. The corresponding beat periods are $\tau_{JJ'} = 2\pi/\omega_{JJ'}$. In Sec. III we compare the results obtained using our three-parameter fits (11) with those of Eq. (12).

III. RESULTS AND DISCUSSION

Figure 1 displays the results for the normalized yield $S(t)$, Eq. (10), as a function of time delay for carbon [panels (a) and (b)] and silicon [panels (c) and (d)]. The experimental results from Ref. [8], obtained from momentum-resolved images for high-energy ($p \geq 0.4$ a.u.) ionized electrons, are shown by blue circles in each panel. They are compared with (i) our analytical formula (11) fitted using t_0, S_b, and ΔS_b as free parameters, and (ii) the phenomenological five-parameter fit Eq. (12) used previously in Refs. [7, 8]. By varying the range of the time shift parameter t_0 in Eq. (11), several locally optimal fits may be achieved, the one with the smallest absolute value of t_0 being the overall best (shown by the solid red line). Figure 2 shows three fits for Ge, using only Eq. (11) and plotted similarly to Fig. 1 (a) and (c). A full list of fitted parameter values is in Table I.

Simulation of the experimental data by means of Eq. (11) for C and Si clearly shows the

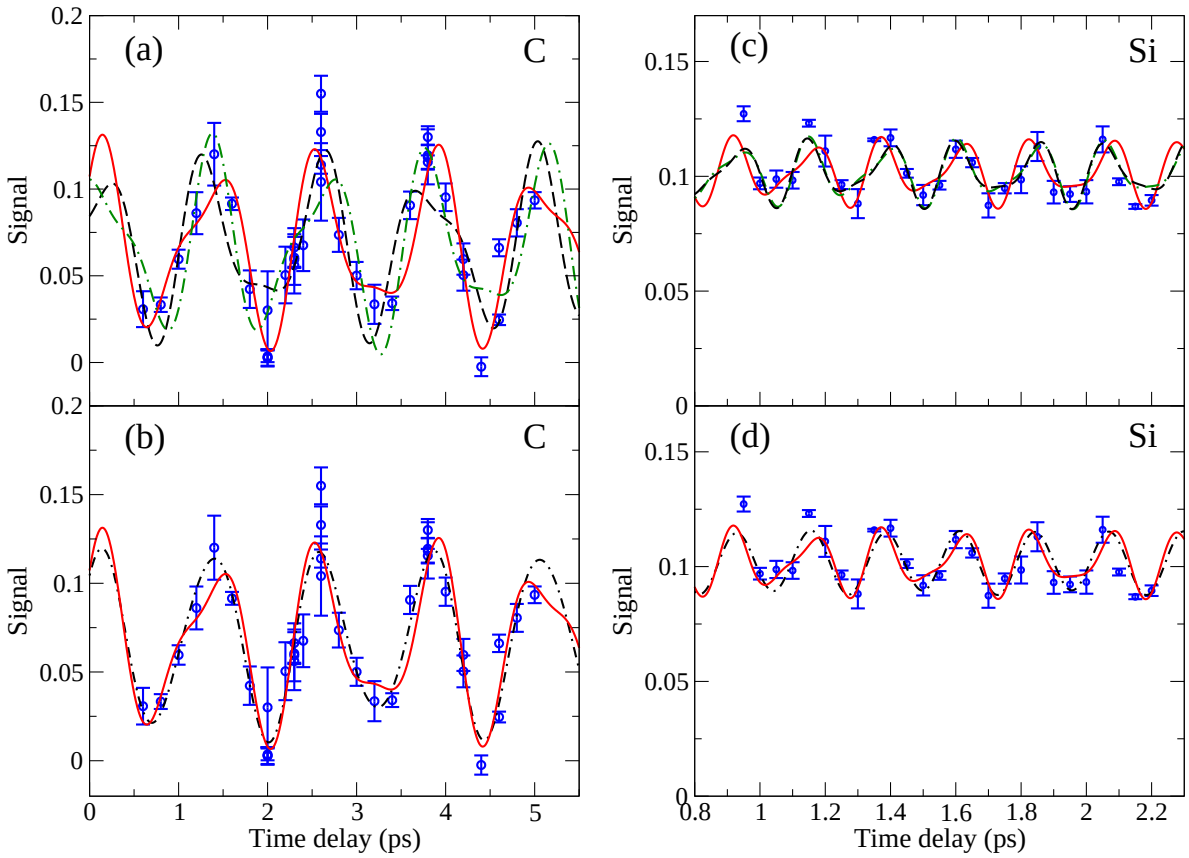

FIG. 1. (Color online) Normalized electron ionization yield as a function of time delay for C [panels (a) and (b)] and Si [panels (c) and (d)]. The graphs in (a) and (c) show several theoretical fits using Eq. (11) with different time shift parameter t_0 that best model the experimental data [8] plotted in blue circles in each panel. The three fits for C in panel (a) correspond to $t_0 = -1.127$ ps (black dashed line), 0.144 ps (red solid line) and 1.381 ps (green dash-dotted line). For Si in panel (c) the fits correspond to $t_0 = -0.213$ ps (black dashed line), 0.013 ps (red solid line) and 0.244 ps (green dash-dotted line). Other parameters are listed in Table I. Panels (b) and (d) compare the best fit from (a) and (c) for C and Si, respectively (red solid line) with the fit obtained by using Eq. (12) [7] (black dash-dotted line).

temporal oscillations originating from quantum beat interference between the coherently populated J sublevels of the ^3P ground state. These oscillations are faster for heavier atoms, as observed in the experiment, which is directly linked to the decrease in the spin-orbit periods $\tau_{JJ'}$ for larger fine-structure splitting energies $\omega_{JJ'}$. As predicted by Eq. (11), the observed beat periods are dominated by the $J = 1$, 2 sublevel contributions with $\tau_{21} =$

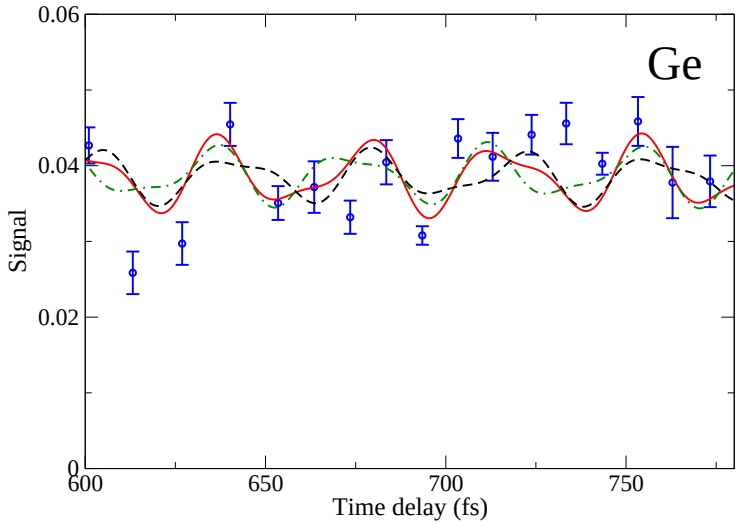

FIG. 2. (Color online) Normalized electron yield as a function of time delay for Ge. Experimental data [8] (blue circles); fits using Eq. (11) correspond to $t_0 = -27.10$ fs (solid red line), 15.66 fs (dashed black line), and 47.98 fs (dash-dotted green line); other parameters are in Table I.

TABLE I. Values of parameters t_0, ΔS_b, and S_b used in Eq. (11) to fit the experimental data from Ref. [8] in Figs. 1 and 2. The χ^2 error representing the quality of the fit for each set of parameters is also shown. The choice of parameters that gives the best fit for each atom is shown in bold.

Atom	Best-fit parameters			Error
	ΔS_b	S_b	t_0 (ps)	χ^2
C	1.11	22.30	−1.127	1.98×10^{-2}
	1.02	**20.96**	**0.144**	$\mathbf{8.89 \times 10^{-3}}$
	0.97	20.45	1.381	1.67×10^{-2}
Si	8.88	90.38	−0.213	1.39×10^{-3}
	8.77	**88.88**	**0.013**	$\mathbf{1.35 \times 10^{-3}}$
	8.85	89.96	0.244	1.38×10^{-3}
Ge	**9.40**	**255.18**	**−0.027**	$\mathbf{4.33 \times 10^{-4}}$
	13.51	362.73	0.016	5.13×10^{-4}
	12.10	324.13	0.048	4.79×10^{-4}

1.24 ps, $\tau_{21} = 0.23$ ps and $\tau_{21} = 39.11$ fs for C, Si, and Ge, respectively.

By introducing the appropriate background parameters in the fits, good agreement with

the experimental data is observed in Fig. 1 for C and Si. The best fits [shown by solid red curves in Fig. 1 (b) and (d)] correspond to the smallest absolute values of t_0 ($\lesssim$ 100 fs), other t_0 values differing from it by $\sim \tau_{21}$. For both atoms, the beat pattern is dominated by the τ_{21} period component, with the τ_{20} beat component producing a characteristic "knee" visible at even half-periods. A similar pattern was observed in numerical simulations for C by Rey and van der Hart [9], but it is totally absent from the fit with the function $f(t)$, Eq. (12), used in the experimental papers [7, 8] [black dash-dotted lines in Fig. 1 (b) and (d)].

For Ge, however, the oscillatory behaviour predicted by Eq. (11) does not provide a good description of the experimental data for any choice of parameters (see Fig. 2). A related feature of the data is that the scale of the oscillations becomes very small in Ge compared with C and Si. This can be seen from the fitted values of S_b and ΔS_b in Table I. From Eq. (11), the time-independent part of the asymmetry is determined by the ratio $\overline{S} = (5/9 + \Delta S_b)/(67/27 + S_b) \sim \Delta S_b/S_b$, while the amplitude of the beats is $\sim 1/S_b$. The data in Figs. 1 and 2, and in Table I show that $\Delta S_b/S_b \sim$ 0.05–0.1 for all three species, while the amplitude of the beats decreases from 0.05 for C, to 0.01 for Si, and 4×10^{-3} for Ge. The latter value is close to the size of error bars in the experimental data for Ge.

This behaviour is related to the effect of the pulse duration in comparison with the beat periods. In the derivation of Eq. (11), the removal of $m = 0$ electrons was assumed to be instantaneous, leading to fully coherent (pure) time-dependent states with wave functions (3) and (7). In the experiment [7, 8] the duration of the pump and probe pulses was 100 fs, which is much shorter the main beat period for C and shorter than that for Si, but is 2.5 times greater than τ_{21} for Ge. As a result, the degree of coherence in the spin-orbit wave packet is largest for C, but becomes progressively smaller in Si and Ge. This results in the reduction of the coherent (oscillatory) part of the signal, with the atomic states produced by the pump becoming closer to a classical ensemble rather than a quantum superposition.

The spin-orbit wave packet in Ge (and to a lesser extent, in Si) is also affected by strong dependence of the multiphoton detachment rates on the threshold energy. This leads to a greater suppression of the detachment probability for higher-lying final atomic states with $J = 1$ and 2, compared with that for the $J = 0$ ground state. The magnitudes of the lowest ($J = 0$) and highest ($J = 2$) thresholds are 1.2621 and 1.2675 eV in C^-, 1.3895 and 1.4172 eV in Si^-, and 1.2327 and 1.4075 eV in Ge^-. Using the method of Ref. [11],

we estimate that for a laser pulse with wavelength $\lambda = 2055$ nm (as in Refs. [7, 8]) and intensity $I = 2 \times 10^{12}$ W/cm^2 (for which the total detachment probability over 100 fs is close to unity), the increase in the threshold energy from the $J = 0$ to $J = 2$ state leads to 2%, 7%, and 40% reduction of the detachment rate, for C, Si, and Ge, respectively. As a result, the contribution of the $J = 2$ state to the wavepacket (1), which is critical for the magnitude of the beats, can be reduced below the values predicted by the LS-coupling coefficients.

The above analysis makes it clear that a complete description of the beat character and spin-orbit coherences of the atomic ensemble requires a density matrix consideration of the problem [2, 5, 12]. Depending on the pump pulse length, strong-field detachment may not generally produce perfectly coherent aligned states. The elements of the density matrix in the $|J, M\rangle$ basis can be determined by calculating the detachment amplitudes for a variety of pulse lengths using existing theory of strong-field photodetachment (e.g., Keldysh-type theory [11, 13–16]). In this approach the diagonal elements will represent populations of different atomic fine-structure levels for a given M, and the magnitude of the off-diagonal elements will describe coherences between the J states. The degree of coherence is then described by the ratio of the off-diagonal elements to the geometric mean of the corresponding diagonal elements. Calculations for the halogen negative ions, whose detachment leads to two fine-structure atomic states, show that the degree of coherence is a function of the ratio $\tau_p/\tau_{JJ'}$, where τ_p is the laser pulse length [12]. For $\tau_p/\tau_{JJ'} \ll 1$ the degree of coherence is close to unity, but it drops quickly for $\tau_p/\tau_{JJ'} \sim 1$ and reaches few-percent values for $\tau_p \approx 2\tau_{JJ'}$, which is similar to the situation in Ge.

IV. CONCLUSIONS

We have investigated the evolution of the ground-state spin-orbit wave packets in carbon, silicon and germanium atoms produced by detachment of $m = 0$ electrons from half-filled valence np^3 negative ions. A simple analytical formula that describes the time-changing alignment of electron orbitals, as probed in the pump-probe experiment, has been derived and applied to the analysis of experimental data [7, 8]. For C and Si the theory provides a good description of temporal beat oscillations which demonstrate the existence of a coherent superposition of the fine-structure sublevels of the atomic triplet state. The sharp

suppression of the coherence degree observed experimentally for Ge demonstrates that the assumption of an instantaneous pulse is insufficient for atoms with shorter beat periods (in the femtosecond range). This calls for a full density-matrix consideration of the problem that would provide a complete description of partially coherent dynamics occurring in spin-orbit manifolds of general atoms with $l \geq 1$ valence electron orbitals.

V. ACKNOWLEDGMENTS

The work of S.M.K.L. has been supported by the Department for Employment and Learning, Northern Ireland. We thank I. Kiyan and M. Eklund for providing experimental data and for useful discussions.

Appendix: Valence-electron states of anions and atoms of C, Si, and Ge

The possible initial states of the $np^3\ {}^4S$ negative ion are

$$|0,0;3/2,3/2\rangle = \boxed{\uparrow}\boxed{\uparrow}\boxed{\uparrow}\,, \tag{A.1}$$

$$|0,0;3/2,1/2\rangle = \frac{1}{\sqrt{3}}\left(\boxed{\uparrow}\boxed{\uparrow}\boxed{\downarrow} + \boxed{\uparrow}\boxed{\downarrow}\boxed{\uparrow} + \boxed{\downarrow}\boxed{\uparrow}\boxed{\uparrow}\right)\,, \tag{A.2}$$

where each of the boxes represents a state of three electrons in the np orbital, with magnetic quantum numbers $m = -1$, 0, and 1, and up ($\uparrow$) or down ($\downarrow$) spins. The states with $M_S = -1/2$ and $-3/2$ are similar and, owing to the symmetry with respect to reflection in the x-y plane, they need not be considered.

The two-electron $np^2\ {}^3P$ states of the neutral atom that can be formed by removal of an $m = 0$ electron from the above states are

$$|1,0;1,1\rangle = \boxed{\uparrow}\boxed{}\boxed{\uparrow}\,, \tag{A.3}$$

$$|1,0;1,0\rangle = \frac{1}{\sqrt{2}}\left(\boxed{\uparrow}\boxed{}\boxed{\downarrow} + \boxed{\downarrow}\boxed{}\boxed{\uparrow}\right)\,, \tag{A.4}$$

or their superposition. Other atomic states that appear in the LS-expansion of the fine-structure levels $|J,M\rangle$ linked to the states (A.3) and (A.4), are

$$|1,1;1,0\rangle = \frac{1}{\sqrt{2}}\left(\boxed{}\boxed{\uparrow}\boxed{\downarrow} + \boxed{}\boxed{\downarrow}\boxed{\uparrow}\right)\,, \tag{A.5}$$

$$|1,-1;1,1\rangle = \boxed{\uparrow}\boxed{\uparrow}\boxed{}\,, \tag{A.6}$$

$$|1,1;1,-1\rangle = \boxed{}\boxed{\downarrow}\boxed{\downarrow}\,. \tag{A.7}$$

Using states (A.3)–(A.7) it is straightforward to work out the relative probabilities of removing $m = 0$ electron by the ionizing probe pulse with polarization parallel to the pump pulse.

For the perpendicular probe polarization, one needs to expand the angular parts of the np electron wave functions $Y_{1m}(\theta, \phi)$ in terms of the spherical functions in a coordinate frame with the z axis perpendicular to the original z axis [17]:

$$Y_{11}(\theta,\phi) = \frac{1}{2}Y_{11}(\tilde{\theta},\tilde{\phi}) - \frac{1}{\sqrt{2}}Y_{10}(\tilde{\theta},\tilde{\phi}) + \frac{1}{2}Y_{1-1}(\tilde{\theta},\tilde{\phi}), \tag{A.8}$$

$$Y_{10}(\theta,\phi) = \frac{1}{\sqrt{2}}Y_{11}(\tilde{\theta},\tilde{\phi}) - \frac{1}{\sqrt{2}}Y_{1-1}(\tilde{\theta},\tilde{\phi}), \tag{A.9}$$

$$Y_{1-1}(\theta,\phi) = \frac{1}{2}Y_{11}(\tilde{\theta},\tilde{\phi}) + \frac{1}{\sqrt{2}}Y_{10}(\tilde{\theta},\tilde{\phi}) + \frac{1}{2}Y_{1-1}(\tilde{\theta},\tilde{\phi}). \tag{A.10}$$

Here $\tilde{\theta}$ and $\tilde{\phi}$ are the polar angles of the new coordinate frame, obtained by rotation through 90 degrees about the original y axis. These formulae show that for the states (A.3) and (A.4) with $M_L = 0$, the average number of $m = 0$ electrons detected in the perpendicular direction is unity, while for the states (A.5)-(A.7) with $M_L = \pm 1$ this number is 0.5. Alternatively, one can expand the fine-structure states $|J, M\rangle$ in Eq. (1) in the frame with the perpendicular z axis using equations similar to (A.8)–(A.10), and analyse the time evolution in it.

[1] L. Young, D. A. Arms, E. M. Dufresne, R. W. Dunford, D. L. Ederer, C. Höhr, E. P. Kanter, B. Krässig, E. C. Landahl, E. R. Peterson, J. Rudati, R. Santra, and S. H. Southworth, Phys. Rev. Lett. **97**, 083601 (2006).

[2] N. Rohringer and R. Santra, Phys. Rev. A **79**, 053402 (2009).

[3] M. A. Lysaght, P. G. Burke, and H. W. van der Hart, Phys. Rev. Lett. **102**, 193001 (2009).

[4] L. Argenti and E. Lindroth, Phys. Rev. Lett. **105**, 053002 (2010).

[5] E. Goulielmakis, Z.-H. Loh, A. Wirth, R. Santra, N. Rohringer, V. S. Yakovlev, S. Zherebtsov, T. Pfeifer, A. M. Azzeer, M. F. Kling, S. R. Leone, and F. Krausz, Nature **466**, 739 (2010).

[6] A. Fleischer, H. J. Wörner, L. Arissian, L. R. Liu, M. Meckel, A. Rippert, R. Dörner, D. M. Villeneuve, P. B. Corkum, and A. Staudte, Phys. Rev. Lett. 107, 113003 (2011).

[7] H. Hultgren, M. Eklund, D. Hanstorp and I. Y. Kiyan, Phys. Rev. A **87**, 031404(R) (2013).

[8] M. Eklund, H. Hultgren, D. Hanstorp and I. Y. Kiyan, Phys. Rev. A **88**, 023423 (2013).

[9] H. F. Rey and H. W. van der Hart, Phys. Rev. A **90**, 033402 (2014).

[10] A. Kramida, Yu. Ralchenko, J. Reader, and NIST ASD Team, NIST Atomic Spectra Database (ver. 5.3), [Online]. Available: `http://physics.nist.gov/asd` [2016, August 16]. National Institute of Standards and Technology, Gaithersburg, MD. (2015).

[11] G. F. Gribakin and M. Yu. Kuchiev, Phys. Rev. A **55**, 3760 (1997).

[12] S. M. K. Law and G. F. Gribakin, (unpublished).

[13] L. V. Keldysh, Zh. Eksp. Teor. Fiz. **47**, 1945 (1964), [Sov. Phys. JETP **20**, 1307 (1965)].

[14] S. F. C. Shearer, M. C. Smyth and G. F. Gribakin, Phys. Rev. A **84**, 033409 (2011).

[15] S. F. C. Shearer and M. R. Monteith, Phys. Rev. A **88**, 033415 (2013).

[16] P. A. Korneev, S. V. Popruzhenko, S. P. Goreslavski, W. Becker, G. G. Paulus, B. Fetić and D. B. Milošević, New J. Phys. **14**, 055019 (2012).

[17] D. A. Varshalovich, A. N. Moskalev and V. K. Khersonskii, *Quantum Theory of Angular Momentum* (World Scientific, Singapore, 1988).